

Laser-Driven Collimated Neutron Sources Based on Kinematic Focusing

P. Liu^{1D},¹ T.Y. Liang^{1D},¹ D. Wu^{2,*},^{*} S.J. Liu,¹ Y.C. Liu^{1D},¹ X. Liu,^{1,2} Z.M. Sheng^{1D},^{1,†} and X.T. He¹

¹*Institute for Fusion Theory and Simulation, Department of Physics, Zhejiang University, Hangzhou 310027, China*

²*Key Laboratory for Laser Plasmas and School of Physics and Astronomy, Collaborative Innovation Center of IFSA (CICIFSA), Shanghai Jiao Tong University, Shanghai 200240, China*



(Received 19 January 2022; revised 26 June 2022; accepted 6 September 2022; published 3 October 2022)

Neutron beams are unique tools to probe samples in many fields, such as biology medicine and fusion research. Access to such sources is traditionally limited to large particle accelerators. However, laser-driven pulsed neutron sources have attracted attention in recent years due to their compactness and cost savings. Although, in practical applications, the major obstacle is terribly low neutron flux due to the isotropic scattering. Here we propose a roadmap for laser-driven neutron sources based on “kinematic focusing,” which is ideal for producing highly collimated neutron beams and leads to the neutron-flux enhancement by more than 1 order of magnitude. Such a good collimation is conducive to the detection of samples located several meters from neutron sources, and it becomes feasible to place sensitive detectors adjacent to the neutron sources without the necessity of heavy shielding. A theoretical model for kinematic focusing and supporting two-dimensional particle-in-cell simulations are presented. It is shown that a well-collimated neutron beam, with the maximal divergence angle of about 30° , is generated by bombardment of a hydrogen target with Li^{3+} beams, which come from a metallic lithium foil irradiated by a short laser pulse at an intensity of $5.5 \times 10^{20} \text{ W cm}^{-2}$. This proposed method can be achieved by present-day petawatt laser facilities.

DOI: 10.1103/PhysRevApplied.18.044004

I. INTRODUCTION

Laser-driven compact neutron sources, as an alternative neutron production method of traditional neutron sources, have been of great research interest for their unique advantages in microscale size, short pulse duration, and low cost. These features are favored by many applications, such as neutron radiography [1], radiation medicine [2], fusion-power-plant material testing [3], and neutron-activation studies. There are two main laser-based paths for neutron productions, i.e., photonuclear reactions [4–7] and beam-target reactions [8–15]. Photonuclear reactions occur as the energetic γ photons from bremsstrahlung radiation of the laser-accelerated electron beams interact with the nucleons. While the beam-target reaction is an approach in which a beam of high-energy (MeV) ions slams onto an appropriate converter and causes nuclear reactions as it slows down inside the material. Neutron sources from beam-target reactions have attracted more attention because of its distinct advantages. On the one hand, neutrons from beam-target reactions usually have high energy and good directionality. On the other hand, the

beam-target reaction cross section is usually several orders of magnitude higher than that of photonuclear. Additionally, schemes of efficient laser-driven ion accelerations, such as radiation pressure acceleration (RPA) [16,17] and breakout afterburner acceleration (BOA) [18,19], provide favorable conditions for the realization of beam-target reactions.

In the past two decades, a large amount of studies of simulation [9–12,15] and experiment [8,13,14,20] on laser-driven neutron production have been conducted based on beam-target configurations. A neutron beam with maximal energy of 18 MeV and a flux of $8 \times 10^8 \text{ n/sr}$ was observed by Higginson *et al.* in an experiment using a laser with peak intensities of $2 \times 10^{19} \text{ W cm}^{-2}$ [13]. Roth *et al.* [14] experimentally reported that energetic neutrons with peak energies up to 70 MeV had also been generated by the employment of a BOA scheme on the TRIDENT laser facility at intensities of $10^{21} \text{ W cm}^{-2}$. However, the emitted neutrons from previous works where light-ion projectiles impinge on heavy-ion secondary targets are distributed at 4π solid angle. Even though the ratio of forward scattering can be improved with the increase of incident beam energy, most neutrons are preferential to be scattered isotropically, which still leads to significant neutron-flux lowering. However, many applications require to deliver

*dwu.phys@sjtu.edu.cn

†zmsheng@zju.edu.cn

a sufficient number of neutrons on targets located several meters from the neutron source [21,22]. Therefore, the collimation of the neutron beams plays a key role because the number of neutrons on targets is determined by the neutron flux rather than the total number of generated neutrons.

Recent experimental studies based on traditional accelerators show that if the projectile is much heavier than the target ion, natural collimation of neutron beams can be achieved [23,24]. Such a collimation is called “kinematic focusing,” which refers to the emission of neutrons at a cone angle here. This is because when a heavy ion is injected to a light-ion target, the system has a large velocity of the center-of-mass (c.m.). Since the neutron production occurs in the c.m. frame, the neutrons are focused kinematically to the forward direction. Whereas there is a drawback of the heavy-ion injection. The beam current from conventional heavy-ion accelerators is much lower than proton accelerators. Therefore, even with the kinematic focusing, it is still difficult to build a neutron generator with a flux comparable with proton drivers. However, the laser-driven ion-acceleration techniques could provide an excellent heavy-ion source for kinematic focusing applications. For one thing, since the effective heavy-ion acceleration using hybrid RPA and target normal sheath acceleration (TNSA) schemes was achieved in a recent experiment [25], the optimal heavy-ion energy for kinematic focusing can be well reached on current laser-plasma accelerators, and for another, the beam current intensity from laser-driven ion sources is extremely high, usually more than 10 orders of magnitude higher than conventional ones.

In this paper, a method of laser-driven highly collimated neutron sources based on kinematic focusing is proposed. We show, through a theoretical model and supporting two-dimensional (2D) particle-in-cell (PIC) simulations, that a well-collimated neutron beam with the maximal divergence angle of about 30° can be generated by bombardment of a hydrogen target with Li³⁺ beams. Such kinematic focusing neutron beams can offer many distinct advantages over the isotropic neutron sources:

- (1) Such a good collimation is conducive to the detection of samples located several centimeters or meters from neutron sources.
- (2) It becomes feasible to place sensitive detectors adjacent to the neutron sources without the necessity of heavy shielding, meaning a reduced irradiation of the experimental devices.

II. THEORETICAL MODEL OF KINEMATIC FOCUSING

In order to well understand the proposed scheme, let us begin with the classical kinematics of a neutron production, which comes from the binary collision between a

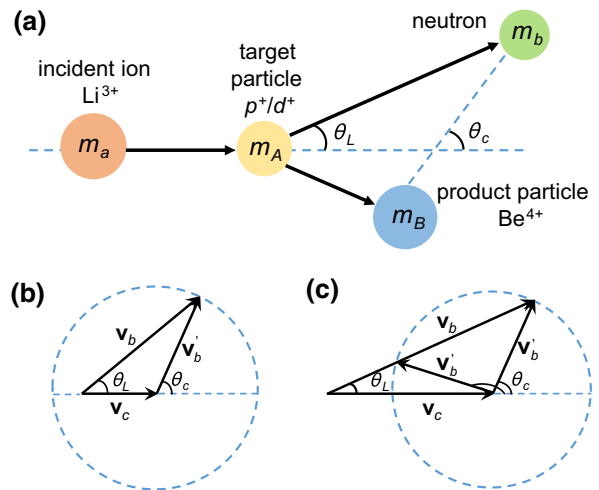


FIG. 1. The diagram of beam-target nuclear reaction where a heavy projectile impinges on a light target nucleus. Angles θ_L and θ_c are the directions of a neutron in the laboratory frame and c.m. frame relative to the direction of the projectile, respectively. (b),(c) Cases of $v_c < v'_b$ and $v_c > v'_b$, where \mathbf{v}_b and \mathbf{v}'_b are, respectively, the neutron velocities in the laboratory frame and c.m. frame, and $\mathbf{v}_c = \mathbf{v}_b - \mathbf{v}'_b$.

projectile particle a with energy of MeV and a static target particle A . In the laboratory frame, as shown in Fig. 1(a), two reactant particles a and A with rest masses m_a and m_A , have a probability to undergo nuclear reaction and create two products, b (here specifically refers to neutrons with rest mass m_b) and B , with an energy gain, Q . For simplicity, we assume particle A is at rest and the momentum of particle a is $m_a \mathbf{v}_a$. In the c.m. frame, the total kinetic energy of these two reactant particles is

$$E' = \frac{1}{2} m_r v_a^2, \quad (1)$$

where $m_r = m_a m_A / (m_a + m_A)$ is the reduced mass. The velocities of the emitted neutron is \mathbf{v}_b and \mathbf{v}'_b in the laboratory frame and c.m. frame, respectively. The relative velocity between them is $\mathbf{v}_c = \mathbf{v}_b - \mathbf{v}'_b$, where the magnitude of \mathbf{v}_c is

$$v_c = \frac{m_r}{m_A} v_a. \quad (2)$$

In the c.m. frame, the Q value of the reaction can be written as

$$Q = \frac{1}{2} m_b v_b'^2 + \frac{1}{2} m_B v_B'^2 - E', \quad (3)$$

where \mathbf{v}'_B and m_B are the velocity and rest mass of resultant nucleus, respectively. It is easy to prove

$$m_b v'_b = m_B v'_B. \quad (4)$$

Combining Eqs. (3) and (4), one can get

$$v'_b = \left[\frac{2m_B}{m_b(m_b + m_B)} (E' + Q) \right]^{1/2}, \quad (5)$$

where $E' \geq |Q|$. For simplicity, we here define a focusing factor

$$\frac{v_c}{v'_b} \equiv \gamma. \quad (6)$$

Substitute Eqs. (1)–(5) into Eq. (6), we have

$$\gamma = \left[\frac{m_a m_b}{m_A m_B} \left(\frac{m_b + m_B}{m_a + m_A} \right) \frac{E'}{E' + Q} \right]^{1/2}. \quad (7)$$

According to the conservation of masses in nuclear reactions, Eq. (7) can therefore be rewritten as

$$\gamma = \left[\left(\frac{m_a m_b}{m_A m_B} \right) \frac{E'}{E' + Q} \right]^{1/2}. \quad (8)$$

Furthermore, according to both energy and momentum conservations of reactants and products, the energy of emitted neutrons is strictly given by [26]

$$E_b = \frac{m_a m_b}{(m_B + m_b)^2} \left\{ \cos \theta_L \pm \left[\cos^2 \theta_L + \frac{m_B m_b}{m_a m_b} \left(m_B - m_a + \frac{m_B}{E_a} Q \right) \right]^{1/2} \right\}^2 E_a, \quad (9)$$

where θ_L is the angle between the neutron velocity and c.m. velocity in the laboratory frame.

According to Eq. (8), for the vast majority of nuclear reactions where the light projectile bombards a heavy target nucleus, one can get $\gamma < 1$. It is found the emitted neutrons gain maximal energy in the direction of incident ion beam, i.e., $\theta_L = 0$, and the minimal energy for the angle of $\theta_L = \pi$. The experiment and simulation results of Refs. [9–15] and references therein are consistent with this theoretical analysis. In the limit of $\gamma \rightarrow 0$, the energy of emitted neutrons remain nearly constant as θ_L varies, which leads to an isotropic emission of neutrons. As shown in Fig. 1(b), one also finds that a divergence angle θ_L is corresponding to only one neutron energy E_b , which means the second term on the right hand of Eq. (9) can only be a positive value.

Equation (8) also implies that for the nuclear reaction of $\gamma > 1$, it must be an endothermic nuclear reaction with a negative Q value. To generate energetic neutrons, the condition that projectiles are heavier than target particles (i.e., $m_a > m_A$) usually needs to be satisfied. Compared with the case of $\gamma < 1$, a divergence angle θ_L is corresponding to two values of neutron energy E_b [see Fig. 1(c)]. Here, one

needs to note that the angle θ_L is now confined to a value with an upper bound of

$$\theta_{L,m} = \arcsin \left(\frac{1}{\gamma} \right). \quad (10)$$

According to Eq. (10), the emitted neutrons can only be confined in the cone angle of $2\theta_{L,m}$, which becomes progressively narrower with the increasing of γ . This model of kinematic focusing points to a useful path for producing collimated neutron beams and therefore achieving high flux.

III. PIC SIMULATION RESULTS

In the following, the 2D PIC simulations are performed to investigate the kinematic focusing of neutrons by using the LAPINS code [27–30], which is based on a high-order implicit numerical scheme and takes advantage of recently developed ionization and collision dynamics models. Recently, a pairwise nuclear-fusion algorithm that fits with pairwise Coulomb scattering was developed in the LAPINS code [30]. Therefore, this code turns out to be an ideal tool for the “first-principles” simulation studies. The whole simulation box is $15 \mu\text{m}$ (z) $\times 40 \mu\text{m}$ (y) with the longitudinal grid resolution of $0.01 \mu\text{m}$ and transverse grid resolution of $0.02 \mu\text{m}$, and each cell is filled with 200 superparticles for both lithium foil and secondary target. A circularly polarized (CP) laser pulse with Gaussian intensity profile $\exp(-r^2/r_0^2)$ is set to propagate along the z axis, where $r_0 = 10\lambda$ is the waist radius with $\lambda = 1 \mu\text{m}$ being the laser wavelength. Here, the dimensionless laser amplitude $a_0 = eE_0/m_e\omega c = 20$ is chosen as a typical example, where E_0 , ω , m_e , e , and c are the electric field amplitude, laser frequency, electron rest mass, electron static charge, and light speed in vacuum, respectively. The laser pulse duration is $\tau = 10T_0$, consisting of a plateau time of $6T_0$ and \sin^2 rising and falling times of $2T_0$, where $T_0 = \lambda/c$ is laser period. The pure lithium and chemical compound of lithium materials such as metallic Li, LiOH, and LiNbO₃ have been successfully applied in the experiment [24], thus in this simulation case the lithium foil is chosen as primary target, which is initially located in the region of $6.0\lambda \leq z \leq 6.1\lambda$ with the mass density of 0.534 gcm^{-3} . The initial ionization degree of lithium is $Z = 1$, corresponding to an electron density $n_e = 41n_c$, where $n_c = \epsilon_0 m_e \omega^2 / e^2$ is the critical density. Then the ionization is fully determined by field ionization and collision ionization.

The ⁷Li(p, n) ⁷Be reaction as a common endothermic one with $Q = -1.644 \text{ MeV}$ is naturally considered, in which the condition of $\gamma > 1$ can be well satisfied according to Eq. (8). In this case, the secondary target, hydrogen plasma, with initial density of $80n_c$ and temperature of 5 eV, is located at $6.3\lambda \leq z \leq 9.3\lambda$. Figures 2(a) and 2(b) show the distributions of particle density and electric field.

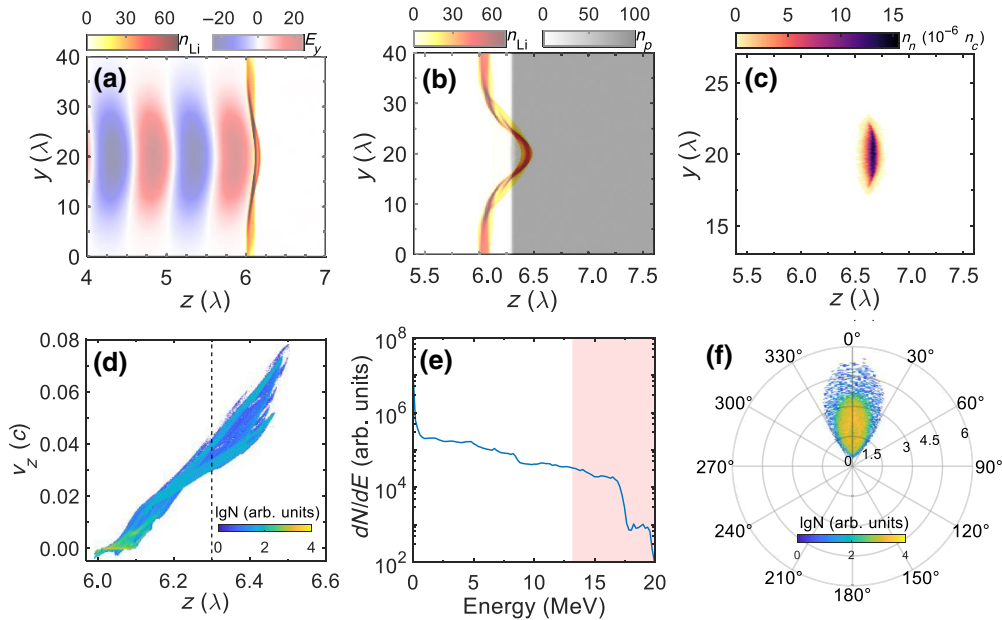


FIG. 2. (a) Spatial distributions of Li^{3+} density (n_{Li}) and transverse electric field (E_y) at $t = 40$ fs. (b), (c) Densities of Li^{3+} (n_{Li}), protons (n_p), and neutrons (n_n) at $t = 60$ fs. Here, the ion density and electric field are normalized to n_c and $m_e \omega c/e$, respectively. Phase-space distribution (d) and energy spectrum (e) of Li^{3+} in Fig. 2(b). Here, the black dashed line indicates the longitudinal position of hydrogen target, the pink shaded area corresponds to Li^{3+} whose energy is greater than the threshold value of ${}^7\text{Li}(p, n) {}^7\text{Be}$ reaction. (f) Energy angular distribution of neutrons at $t = 60$ fs, where the radius represents the neutron energy in units of MeV.

One can see that, at the time $t = 40$ fs, when a circularly polarized laser normally irradiates the front surface of lithium foil, almost all lithium ions are fully ionized and pushed forward. Subsequently, at $t = 60$ fs, the Li^{3+} beam is accelerated by light pressure stably, which is a typical light-sail acceleration (LSA) process [17]. By this moment the lithium foil is compressed reaching the density of $n_{\text{Li}} \simeq 51n_c$, meaning a high beam current intensity. Such a high-density beam bombarding hydrogen plasma is extremely useful to improve the reactivity. It should be remarked that laser pulse has been reflected away by the thick hydrogen target by this time ($t = 60$ fs), which therefore avoids the instability of the laser-foil interactions in the later stage of LSA [17,31]. Therefore, it is relatively easy to achieve a LSA in this scenario due to the short interaction time (10–20 fs) and low ion energy requirement (13–50 MeV).

From the phase-space ($z - p_z$) map and energy spectrum of Li^{3+} beam in Figs. 2(d) and 2(e), we can observe that the lithium ions have collided with the hydrogen plasma at $t = 60$ fs. The fastest ions have already transported into a depth of about 0.2λ with energies of about 20 MeV, which is larger than the threshold value E_{th} of ${}^7\text{Li}(p, n) {}^7\text{Be}$ reaction. Here, $E_{\text{th}} = -Q(m_{\text{Li}} + m_p)/m_p = 13.152$ MeV. As Li^{3+} particles slow down in the hydrogen plasma, the nuclear reactions are triggered, the possible reactions for neutron productions are summarized in Table I [23]. Since the energy of lithium ions in our simulations is

always lower than 49.7 MeV, the last exit channel is negligible.

The simulated neutron density map and their energy angular distributions are shown in Figs. 2(c) and 2(f), respectively. From Fig. 2(c), one can see that, at the moment $t = 60$ fs, a compact neutron beam is generated with maximal energy of about 5.24 MeV, which can be predicted by Eq. (9). Though the pulse duration of neutrons inevitably becomes larger over time, the neutron beam still moves forwards as a whole. Compared with the results of most of the previous literature [9–15], the neutron beam in our work is highly collimated. For the scenario considered in Fig. 2, the maximal divergence angle defined by Eq. (10) is $\theta_{L,m} = 35.7^\circ$, which is in good agreement with the value 36.6° obtained in the simulation, as shown in Fig. 2(f). It is found that the vast majority of neutrons are concentrated in a divergence angle between about -30° and 30° , and

TABLE I. The main nuclear reaction channels of ${}^7\text{Li}(p, n) {}^7\text{Be}$ [23]. Here, E_{th} and σ_p represent the threshold value and peak cross section of reactions, respectively.

Type of exit channel	Q value (MeV)	E_{th} (MeV)	σ_p (mb)
$n + {}^7\text{Be}$	−1.644	13.152	580
$n + {}^7\text{Be} *$ (0.429 MeV)	−2.073	16.584	60
$n + {}^7\text{Be} *$ (4.57 MeV)	−6.214	49.712	—

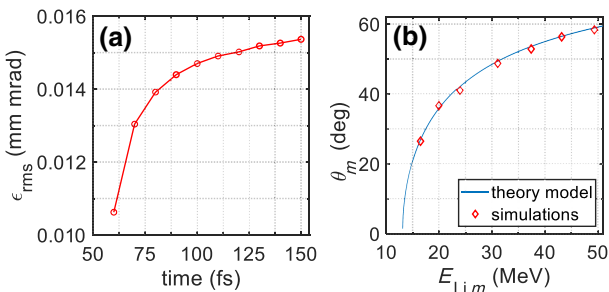


FIG. 3. (a) Temporal evolution of rms emittance ϵ_{rms} for neutron beam in the ${}^7\text{Li}(p, n){}^7\text{Be}$ reaction case. (b) The relationship between θ_m and $E_{\text{Li},m}$. The red diamonds represent the simulation results by the LAPINS code. The blue solid line is obtained from Eq. (10).

the corresponding solid angle is $\Omega = 0.268\pi$, which leads to the neutron-flux enhancement by more than 1 order of magnitude compared with the conventional reactions with a proton beam bombarding a lithium target.

Furthermore, we also calculate the normalized transverse rms emittance of this neutron beam, which is defined as $\epsilon_{\text{rms}} = (\langle y^2 \rangle \langle p_y^2 \rangle - \langle y p_y \rangle^2)^{1/2} / m_b c$ [32], where $\langle \cdot \rangle$ represents averaging over beam distributions. The evolution of the emittance is shown in Fig. 3(a). One can see that the ϵ_{rms} increases sharply at an early stage and then a saturation stage is followed. At the end of simulation, the emittance of this neutron beam is only 0.0154 mm mrad, which indicates a good directionality. The rms emittance from the

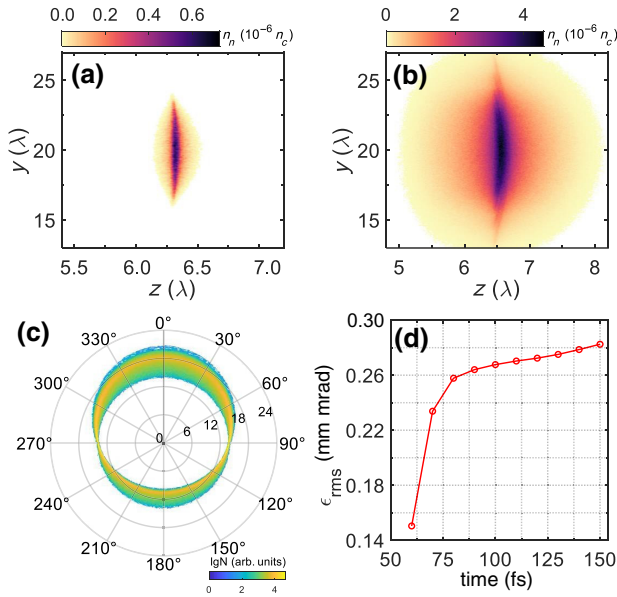


FIG. 4. Simulations results of the $d({}^7\text{Li}, n){}^8\text{Be}$ reaction. Snapshots of neutron density at two times of $t = 60$ fs (a) and $t = 90$ fs (b). (c) Energy angular distribution of neutrons at $t = 60$ fs. Here, the radius gives the neutron energy in MeV. (d) Temporal evolution of ϵ_{rms} for neutrons.

conventional case of proton-beam impinging on lithium target is also computed, and we find it is about 1 order of magnitude higher than that in the kinematic focusing case.

Besides this typical example, we also scan in a wide range of maximal energy of Li^{3+} beam (i.e., corresponding to different laser intensities) to show the validity of this theoretical model. Figure 3(b) plots the relationship between maximal divergence angle θ_m and the maximal energy $E_{\text{Li},m}$ obtained from PIC simulations by fixing other parameters. We see that the results from simulations are always in agreement with those predicted by Eq. (10). It is noted that to produce lithium ions with optimal energies is key to generate high flux neutron sources with small divergence angle.

It is noteworthy that, from this theoretical model [Eq. (8)], the kinematic focusing is not only dependent on the mass of projectiles and targets but also strongly related to the Q value. Therefore, for the reaction ${}^7\text{Li} + d \rightarrow {}^8\text{Be} + n$ ($Q = 15.03$ MeV) [12], even though light deuterons are bombarded by heavy lithium ions, it is impossible to realize kinematic focusing due to $\gamma < 1$, which is also verified by our 2D PIC simulations. In this simulation, by keeping the other parameters the same, a

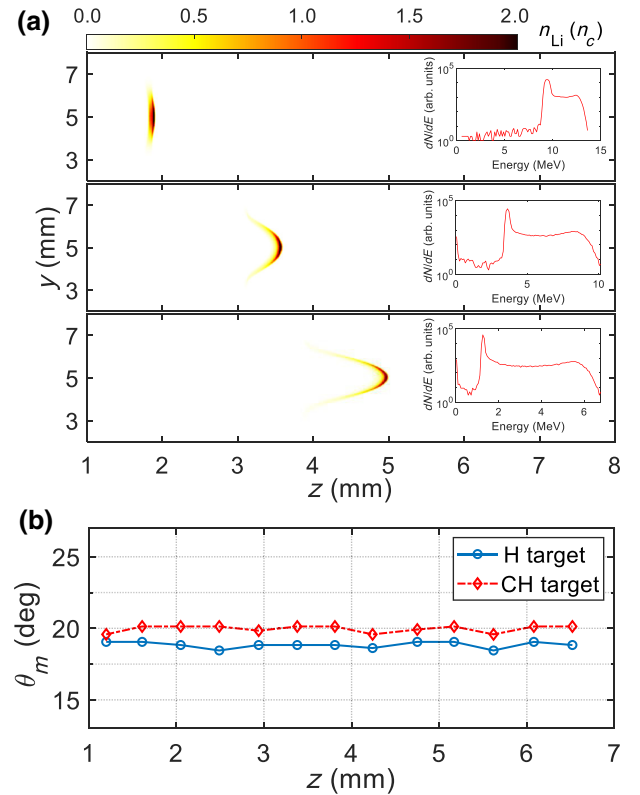


FIG. 5. Transport process of particle beams in large-scale plasma. (a) Snapshots of Li^{3+} density and corresponding energy spectrum at three times: $t = 100$ ps, $t = 200$ ps, and $t = 300$ ps (from top to bottom). (b) Spatial evolution of θ_m for neutron beam.

CP laser with $a_0 = 15$ and deuterium plasma with initial density of $n_d = 80n_c$ are employed. As shown in Figs. 4(a) and 4(b), one can see that, during the period of $t \in [60 \text{ fs}, 90 \text{ fs}]$, neutrons from this case move in all directions simultaneously, and they are distributed throughout the polar angle [see Fig. 4(c)], which shows significant differences from the $^7\text{Li}(p, n)^7\text{Be}$ reaction case [Fig. 2(f)]. Similarly, we also display the rms emittance of neutron beam in Fig. 4(d), and it is found that the ϵ_{rms} is 1 order of magnitude larger than that in the kinematic focusing case [Fig. 3(a)].

IV. DISCUSSION AND CONCLUSION

Note that the LAPINS code is based on a high-order implicit numerical algorithm, which eliminates the numerical cooling found in the standard implicit PIC methods by using a pseudo-electric-field method [29]. Thus this method is more time saving and can suppress numerical instabilities. Based on these advantages, it now has the ability to study the processes of large-scale beam-plasma interactions [33], and it can even simulate some plasma phenomena that are achieved by the hybrid fluid-PIC program [34]. Figure 5(a) shows the evolutions of Li^{3+} beam density and the corresponding energy spectrum as it transports in hydrogen plasma of several millimeters. In order to highlight the influence of target ion scattering on neutron divergence in large-scale plasma, the electromagnetic field effects are not taken into account in this example. Here we analyze the propagation of neutrons in both pure hydrogen target and mixed hydrocarbon target ($\text{C} : \text{H} = 1 : 1$), and the evolutions of the neutron divergence angles for these two cases are shown in Fig. 5(b), it is found that the θ_m remains around 20° . Compared with the case of the pure hydrogen target, the divergence angles in the case of hydrocarbon target increase slightly. But in short, the neutron beam can keep good collimation after propagating a distance of several millimeters.

It should also be pointed out that in addition to using the solid plastic targets mentioned above as the secondary target materials, gas jet plasma can also be employed because the total yield of neutrons is proportional to the area density of the target, that is to say, when the length of gas jet plasma targets is long enough, sufficient neutrons can be produced even if its density is relatively low.

In conclusion, a method of laser-driven neutron production, which is based on kinematic focusing scheme, is proposed. Supported by theoretical model and 2D PIC simulations with kinematic nuclear reactions, it is found that a well-collimated neutron beam with the maximal divergence angle of about 30° and solid angle of $\Omega = 0.268\pi$ can be generated by bombardment of a hydrogen target with Li^{3+} beams, which come from a metallic lithium foil irradiated by a short laser pulse at intensities of $5.5 \times 10^{20} \text{ W cm}^{-2}$. This proposed method can be well achieved

by current petawatt laser facilities and, thus, might unblock the path to high flux neutron sources.

ACKNOWLEDGMENTS

This work is supported by the National Natural Science Foundation of China (Grants No. 12075204, No. 11875235, and No. 61627901), the Strategic Priority Research Program of Chinese Academy of Sciences (Grant No. XDA250050500) and Shanghai Municipal Science and Technology Key Project (No. 22JC1401500). Dong Wu thanks the sponsorship from Yangyang Development Fund.

- [1] K. L. Lancaster, S. Karsch, H. Habara, F. N. Beg, E. L. Clark, R. Freeman, M. H. Key, J. A. King, R. Kodama, K. Krushelnick, K. W. D. Ledingham, P. McKenna, C. D. Murphy, P. A. Norreys, R. Stephens, C. Stoeckl, Y. Toyama, M. S. Wei, and M. Zepf, Characterization of $^7\text{Li}(p, n)^7\text{Be}$ neutron yields from laser produced ion beams for fast neutron radiography, *Phys. Plasmas* **11**, 3404 (2004).
- [2] A. Wittig, J. Michel, R. L. Moss, F. Stecher-Rasmussen, H. F. Arlinghaus, P. Bendel, P. L. Mauri, S. Altieri, R. Hilger, P. A. Salvadori, L. Menichetti, R. Zamenhof, and W. A. Sauerwein, Boron analysis and boron imaging in biological materials for boron neutron capture therapy (BNCT), *Crit. Rev. Oncol. Hematol.* **68**, 66 (2008).
- [3] L. J. Perkins, B. G. Logan, M. D. Rosen, M. D. Perry, T. D. de la Rubia, N. M. Ghoniem, T. Ditmire, P. T. Springer, and S. C. Wilks, The investigation of high intensity laser driven micro neutron sources for fusion materials research at high fluence, *Nucl. Fusion* **40**, 1 (2000).
- [4] K. W. D. Ledingham, *et al.*, Photonuclear Physics when a Multiterawatt Laser Pulse Interacts with Solid Targets, *Phys. Rev. Lett.* **84**, 899 (2000).
- [5] X. J. Jiao, J. M. Shaw, T. Wang, X. M. Wang, H. Tsai, P. Poth, I. Pomerantz, L. A. Labun, T. Toncian, M. C. Downer, and B. M. Hegelich, A tabletop, ultrashort pulse photoneutron source driven by electrons from laser wakefield acceleration, *Matter Radiat. Extremes* **2**, 296 (2017).
- [6] X. R. Jiang, D. B. Zou, Z. J. Zhao, L. X. Hu, P. Han, J. Q. Yu, T. P. Yu, Y. Yin, and F. Q. Shao, Microstructure-Assisted Laser-Driven Photonuclear Pulsed Neutron Source, *Phys. Rev. Appl.* **15**, 034032 (2021).
- [7] I. Pomerantz, E. McCary, A. R. Meadows, A. Arefiev, A. C. Bernstein, C. Chester, J. Cortez, M. E. Donovan, G. Dyer, E. W. Gaul, D. Hamilton, D. Kuk, A. C. Lestrade, C. Wang, T. Ditmire, and B. M. Hegelich, Ultrashort Pulsed Neutron Source, *Phys. Rev. Lett.* **113**, 184801 (2014).
- [8] L. Disdier, J.-P. Garçonnet, G. Malka, and J.-L. Miquel, Fast Neutron Emission from a High-Energy Ion Beam Produced by a High-Intensity Subpicosecond Laser Pulse, *Phys. Rev. Lett.* **82**, 1454 (1999).
- [9] J. Davis, and G. M. Petrov, Angular distribution of neutrons from high-intensity laser-target interactions, *Plasma Phys. Controlled Fusion* **50**, 065016 (2008).

- [10] G. M. Petrov, and J. Davis, Neutron production from interactions of high-intensity ultrashort pulse laser with a planar deuterated polyethylene target, *Phys. Plasmas* **15**, 073109 (2008).
- [11] J. Davis, G. M. Petrov, T. Petrova, L. Willingale, A. Mak-simchuk, and K. Krushelnick, Neutron production from $^7\text{Li}(d, xn)$ nuclear fusion reactions driven by high-intensity laser-target interactions, *Plasma Phys. Controlled Fusion* **52**, 045015 (2010).
- [12] G. M. Petrov, D. P. Higginson, J. Davis, T. B. Petrova, C. McGuffey, B. Qiao, and F. N. Beg, Generation of energetic (>15 MeV) neutron beams from proton- and deuteron-driven nuclear reactions using short pulse lasers, *Plasma Phys. Controlled Fusion* **55**, 105009 (2013).
- [13] D. P. Higginson, J. M. McNamey, D. C. Swift, G. M. Petrov, J. Davis, J. A. Frenje, L. C. Jarrott, R. Kodama, K. L. Lancaster, A. J. Mackinnon, H. Nakamura, P. K. Patel, G. Tynan, and F. N. Beg, Production of neutrons up to 18 MeV in high-intensity, short-pulse laser matter interactions, *Phys. Plasmas* **18**, 100703 (2011).
- [14] M. Roth, *et al.*, Bright Laser-Driven Neutron Source Based on the Relativistic Transparency of Solids, *Phys. Rev. Lett.* **110**, 044802 (2013).
- [15] X. R. Jiang, F. Q. Shao, D. B. Zou, M. Y. Yu, L. X. Hu, X. Y. Guo, T. W. Huang, H. Zhang, S. Z. Wu, G. B. Zhang, T. P. Yu, Y. Yin, H. B. Zhuo, and C. T. Zhou, Energetic deuterium-ion beams and neutron source driven by multiple-laser interaction with pitcher-catcher target, *Nucl. Fusion* **60**, 076019 (2020).
- [16] T. Esirkepov, M. Borghesi, S. V. Bulanov, G. Mourou, and T. Tajima, Highly Efficient Relativistic-Ion Generation in the Laser-Piston Regime, *Phys. Rev. Lett.* **92**, 175003 (2004).
- [17] A. P. L. Robinson, M. Zepf, S. Kar, R. G. Evans, and C. Bellei, Radiation pressure acceleration of thin foils with circularly polarized laser pulses, *New J. Phys.* **10**, 013021 (2008).
- [18] L. Yin, B. J. Albright, B. M. Hegelich, K. J. Bowers, K. A. Flippo, T. J. T. Kwan, and J. C. Fernández, Monoenergetic and GeV ion acceleration from the laser breakout afterburner using ultrathin targets, *Phys. Plasmas* **14**, 056706 (2007).
- [19] L. Yin, B. J. Albright, K. J. Bowers, D. Jung, J. C. Fernández, and B. M. Hegelich, Three-Dimensional Dynamics of Breakout Afterburner Ion Acceleration Using High-Contrast Short-Pulse Laser and Nanoscale Targets, *Phys. Rev. Lett.* **107**, 045003 (2011).
- [20] K. Mima, A. Yogo, S. R. Mirfayzi, Z. Lan, Y. Arikawa, Y. Abe, and H. Nishimura, Laser-driven neutron source and nuclear resonance absorption imaging at ILE, Osaka University: review, *Appl. Opt.* **61**, 2398 (2022).
- [21] J. G. Fantidis, G. E. Nicolaou, and N. F. Tsagas, Optimization study of a transportable neutron radiography unit based on a compact neutron generator, *Nuclear Instrum. Methods Phys. Res. A, Detectors and Associated Equipment* **618**, 331 (2010).
- [22] Y. Kawabata, T. Nakano, M. Hino, H. Sunohara, U. Matsumura, and N. Takenaka, High contrast neutron radiography with optical devices in Kyoto University reactor, *Nucl. Instrum. Methods Phys. Res. Sect. A* **529**, 238 (2004).
- [23] M. Lebois, J. N. Wilson, P. Halipré, B. Leniau, I. Matea, A. Oberstedt, S. Oberstedt, and D. Verney, Development of a kinematically focused neutron source with the $p(^7\text{Li}, n)^7\text{Be}$ inverse reaction, *Nucl. Instrum. Methods Phys. Res., Sect. A* **735**, 145 (2014).
- [24] S. Ikeda, M. Okamura, T. Kanesue, D. Raparia, A. Hershcovitch, K. Yip, K. Takahashi, D. Wu, A. Cannavó, and G. Ceccio, Neutron generator based on intense lithium beam driver, *Rev. Sci. Instrum.* **91**, 023304 (2020).
- [25] W. J. Ma, *et al.*, Laser Acceleration of Highly Energetic Carbon Ions Using a Double-Layer Target Composed of Slightly Underdense Plasma and Ultrathin Foil, *Phys. Rev. Lett.* **122**, 014803 (2019).
- [26] N. Izumi, Y. Sentoku, H. Habara, K. Takahashi, F. Ohtani, T. Sonomoto, R. Kodama, T. Norimitsu, H. Fujita, Y. Kitagawa, K. Mima, K. A. Tanaka, and T. Yamanaka, Observation of neutron spectrum produced by fast deuterons via ultra-intense laser plasma interactions, *Phys. Rev. E* **65**, 036413 (2002).
- [27] D. Wu, X. T. He, W. Yu, and S. Fritzsche, Monte Carlo approach to calculate proton stopping in warm dense matter within particle-in-cell simulations, *Phys. Rev. E* **95**, 023207 (2017).
- [28] D. Wu, X. T. He, W. Yu, and S. Fritzsche, Monte Carlo approach to calculate ionization dynamics of hot solid-density plasmas within particle-in-cell simulations, *Phys. Rev. E* **95**, 023208 (2017).
- [29] D. Wu, W. Yu, S. Fritzsche, and X. T. He, High-order implicit particle-in-cell method for plasma simulations at solid densities, *Phys. Rev. E* **100**, 013207 (2019).
- [30] D. Wu, Z. M. Sheng, W. Yu, S. Fritzsche, and X. T. He, A pairwise nuclear fusion algorithm for particle-in-cell simulations: Weighted particles at relativistic energies, *AIP Adv.* **11**, 075003 (2021).
- [31] T.-P. Yu, A. Pukhov, G. Shvets, and M. Chen, Stable Laser-Driven Proton Beam Acceleration from a Two-Ion-Species Ultrathin Foil, *Phys. Rev. Lett.* **105**, 065002 (2010).
- [32] K. Floettmann, Some basic features of the beam emittance, *Phys. Rev. ST Accel. Beams* **6**, 034202 (2003).
- [33] B. Z. Chen, D. Wu, J. R. Ren, D. H. H. Hoffmann, and Y. T. Zhao, Transport of intense particle beams in large-scale plasmas, *Phys. Rev. E* **101**, 051203 (2020).
- [34] H. B. Cai, X. X. Yan, P. L. Yao, and S. P. Zhu, Hybrid fluid-particle modeling of shock-driven hydrodynamic instabilities in a plasma, *Matter Radiat. Extremes* **6**, 035901 (2021).